Imaging and Radiation Research (2020) Volume 3 Issue 1
doi:10.24294/irr.v3i1.1727

REVIEW ARTICLE

Trends and developments in cardiac magnetic resonance imaging

Andreas Mayr[1], Günter Reiter[2], Dietrich Beitzke[3*]

[1] *Universitätsklinik für Radiologie, Medizinische Universität Innsbruck, Innsbruck, Austria.*

[2] *Research and Development, Siemens Healthcare Diagnostics GmbH, Graz, Austria.*

[3*] *Universitätsklinik für Radiologie und Nuklearmedizin, Medizinische Universität Wien, Wien, Austria. E-mail: dietrich.beitzke@meduniwien.ac.at*

ABSTRACT

Background: Through the development of robust techniques and their comprehensive validation, cardiac magnetic resonance imaging (CMR) has developed a wide range of indications in its almost 25 years of clinical use. The recording of cardiac volumes and systolic ventricular function as well as the characterization of focal myocardial scars are now part of standard CMR imaging. Recently, the introduction of accelerated image acquisition technologies, the new imaging methods of myocardial T1 and T2 mapping and 4-D flow measurements, and the new post-processing technique of myocardial feature tracking have gained relevance. **Method:** This overview is based on a comprehensive literature search in the PubMed database on new CMR techniques and their clinical application. **Results and conclusion:** This article provides an overview of the latest technical developments in the field of CMR and their possible applications based on the most important clinical questions.

Keywords: T1 Mapping; 4-D Flow Measurements; Myocardial Storage Diseases; Myocarditis; Compressed Sensing

ARTICLE INFO

Received: 26 August 2020
Accepted: 24 October 2020
Available online: 6 November 2020

1. Introduction

Recent developments in cardiac magnetic resonance (CMR) imaging have recently overcome some limitations of conventional, established CMR sequences. Accelerated image acquisition techniques such as “compressed sensing”, the possibility of absolute quantification of even diffuse myocardial changes by means of myocardial mapping, or new post-processing applications such as “strain imaging” expand the efficiency and clinical utility of CMR in a variety of cardiac diseases[1]. Meanwhile, 54% of all guidelines of the European Society of Cardiology (ESC Guidelines) contain recommendations for the use of CMR[2].

2. Latest technical developments

2.1 Accelerated image reconstruction

For the CMR images acquired in a segmented, time-synchronized manner, a portion of the required k-space lines is acquired in each case in different heartbeats during a breath-hold phase in an ECG-synchronized manner. This technique is especially sensitive to arrhythmias and breath-hold problems. Approaches developed in recent years to shorten CMR image acquisition are based on reconstructing a full image from previous, highly unsampled, but multiple coil element acquired data information in k-space. Parallel imaging techniques of co-

mmercial magnetic resonance imaging (MRI) systems such as Sensitivity Encoding (Sense) and Generalized Autocalibrating Partial Parallel Acquisition (Grappa), are typically limited to a 2- to 3-fold acceleration. The innovative Compressed-sensing (CS) technique enables image reconstruction from even significantly fewer lines of data by compressing the information content of CMR images ("sparsity") and eliminating noise-like image reconstruction artifacts through iterative image reconstruction[3]. The CS technique finds application in various sequences, including perfusion imaging[4], real-time cine imaging under free breathing[5] (**Figure 1**), phase contrast flow measurement[6], 3-D late gadolinium enhancement[7], and T1 mapping[8]. Recent work has also demonstrated the use of CS in the free-breathing radial technique for continuous recordings[9]; where data can be separated into both cardiac and respiratory dimensions without the need for cardiac gating or breath-holding. The increasing availability of improved computer hardware now makes these computationally intensive reconstruction methods practical. With numerous studies demonstrating the robustness of CS techniques for routine clinical use, these methods are being made available in current generations of commercial MRI systems.

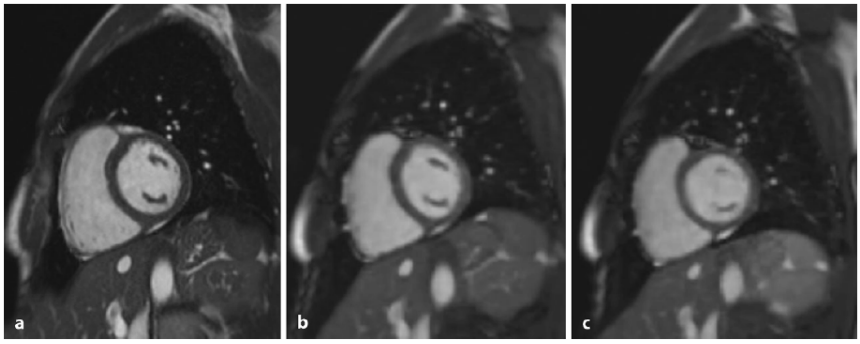

Figure 1. Cine imaging with "compressed sensing".
Note: Image comparison between a standard short-axis slice in breath-hold technique (11 times to cover the left ventricle) (**a**); accelerated imaging "compressed sensing" with 2 breath-holds per left ventricle (**b**, **c**); singular breath-hold to cover the left ventricle. Compared to conventional technique, the accelerated sequences show a slightly increased image noise while maintaining diagnostic image quality.

2.2 Advanced myocardial characterization

The late gadolinium enhancement (LGE) technique is the most established CMR method for characterizing focal myocardial changes[10]. The T1-weighted sequences used differentiate ischemic from nonischemic pathologies with high diagnostic accuracy based on the gadolinium distribution pattern in the extracellular myocardial compartment and provide relevant prognostic information[11]. Major drawbacks of this technique include the inability to distinguish between acute and chronic changes and to detect diffuser myocardial damage. As the most exciting CMR innovation, the myocardial "mapping" techniques recently introduced into routine clinical practice, with their absolute quantificability of magnetic tissue properties, offer decisive advantages in the characterization of early preclinical to terminal stages of myocardial disease[12].

2.2.1 T1 mapping and extracellular volume fraction

Myocardial T1 mapping maps the T1 relaxation time (longitudinal relaxation) of each myocardial pixel by acquiring multiple inversion or saturation recovery images[12]. Among the most widespread and common sequences are the modified look-locker inversion recovery sequence (MOLLI)[13] and its further development ("short" MOLLI)[14], which can shorten the duration of breath-hold. In the typically automatically calculated T1 maps of the myocardium, the pixel-by-pixel myocardial T1 relaxation times are the result of the proportion of myocytes and interstitium in the pixel. Pathophysiologic processes such as diffuse interstitial fibrosis, myocardial edema, or

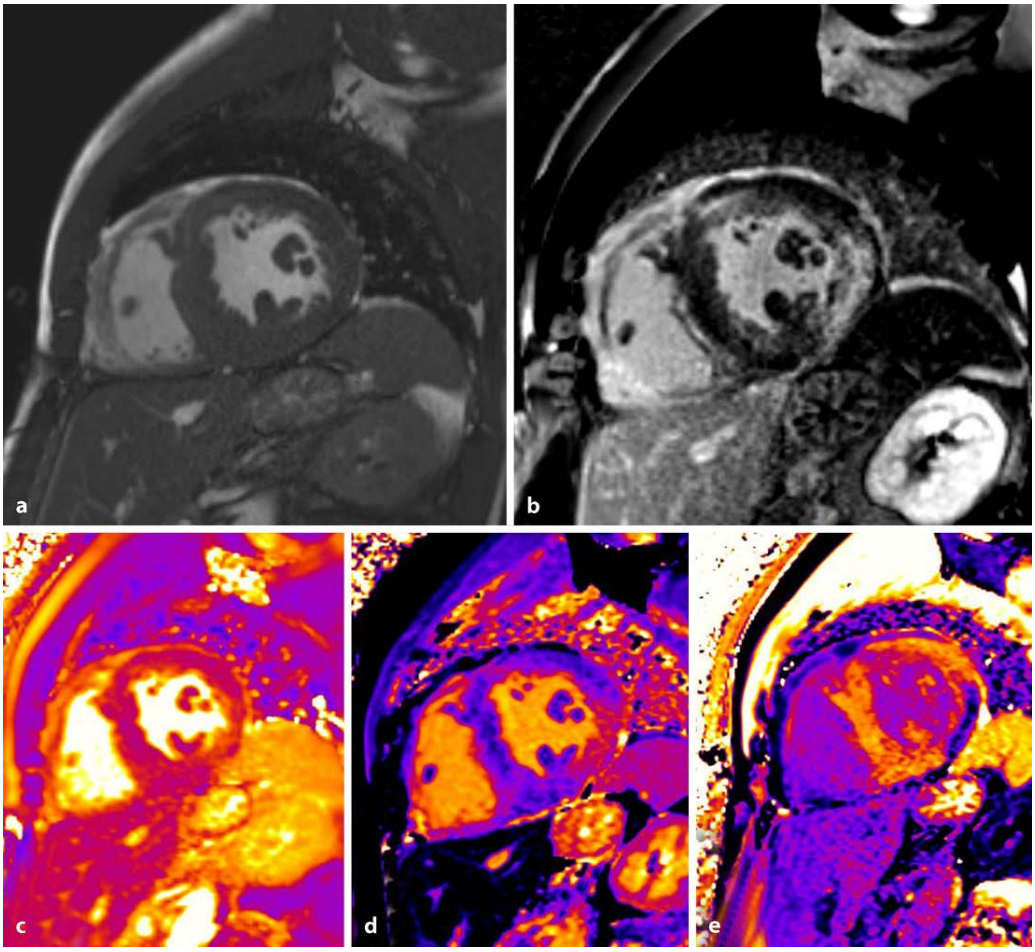

Figure 2. Fabry disease.
(**a**): Multiparametric cardiac magnetic resonance imaging (MRI) of a 65-year-old male patient with newly detected left ventricular hypertrophy; (**b**): late gadolinium enhancement (LGE) shows extensive scarring in the lateral wall region, also visible in T1 mapping (**d**) and post-contrast T1 map/ECV (extracellular volume fraction). The remaining left ventricle shows significantly decreased T1 values (~ 850 ms) in T1 mapping (**d**). The T2 map (**c**) shows slightly increased values in the sense of minor edema in the lateral wall. The ECV map (**e**) also clearly shows scarring in the lateral wall. The changes are typical for an advanced stage of Fabry disease. The decreased values originate from the glycosphingolipid deposits (fat).

amyloid deposition are characterized by increases in T1 relaxation times, whereas glycosphingolipid depletion in the setting of Fabry disease (**Figure 2**) or myocardial egg overloads result in characteristic T1 relaxation time reductions[15]. The consensus statement of the Society for Cardiovascular Magnet Resonance Imaging (SCMR) recommends the primary use of local reference values even for commercially available pulse sequences[12,16].

The evaluation of diffuse diseases should be performed by measuring the ROI ("region of interest") in the midventricular septum of short-axis images; in the case of focal myocardial processes, additional ROIs should be provided in areas with visually abnormal appearance[16].

While native T1 relaxation time represents a composite myocardial signal of myocytes and interstitium and alone cannot fully differentiate the underlying disease process (fibrosis, edema, amyloid, and/or myocyte necrosis)[17], myocardial extracellular volume fraction (ECV) represents another parameter determinable by T1 mapping. Calculation of ECV requires measurement of T1 relaxation time of myocardium and blood before and after the administration of the contrast medium. In addition, the daily updated hematocrit value should be available, but alternatively, a synthetic ECV can be calculated using a hematocrit estimation based on native T1 values of the blood[16]. Contrast T1 mapping data can be acquired at least 10 to 30 minutes after contrast application in order to achieve the balance of contrast concentrations between blood and inter-

stitium required for ECV calculation[10]. ECV standard values of healthy subjects are 25 ± 4% in 1.5-T-MRI and 27 ± 1% in 3-T-MRI[18]. Increases in ECV are mainly caused by excessive collagen deposition in the context of myocardial fibrose or amyloid deposition, especially in the transthyretin (ATTR) amyloidosis subtype[15].

2.2.2 T2 mapping

The challenges of the conventional T2-weighted short-tau inversion recovery (T2-STIR) sequence, which has been most commonly used for CMR edema detection, include artifacts, the intrinsically low contrast-to-noise ratio compared to LGE sequences, and the only qualitative or semiquantitative approach of this technique[19]. Using T2 mapping, myocardial T2 relaxation times can be quantified pixel-by-pixel as a surrogate of myocardial water content; moreover, T2 mapping is considered the most reproducible of all CMR techniques for myocardial edema detection[20]. Analogous to T1 mapping, acquisition of local reference values is recommended; published normal values of T2 relaxation times using balanced steady-state free precession (bSSFP) techniques are 52 ± 3 ms on 1.5-T-MRI and 45 ms on 3-T-MRI[21,22]. Significant published evidence and partial guidelines suggest the use of T2 mapping for the following clinical indications: myocarditis, myocardial infarction, sarcoid dose, cardiac transplant rejection, and chemotoxic cardiomyopathy.

2.3 4-D flow measurements in the heart and great vessels

In contrast to 2-D phase-contrast flow measurements, which are established components of clinical CMR examinations[23], 4-D flow measurements (i.e., time-resolved, ECG-triggered recordings of not only unidirectional but all 3 velocity components) allow a much more detailed analysis of macroscopic cardiovascular flow mechanics.

The acquisition strategy of 4-D flow measurements typically consists of acquiring the complete temporally varying velocity field within a volume of interest under free breathing (**Figure 3**). This can be done either in the form of 2-D multilayer cine phase contrast measurements or a 3-D spatial cine phase contrast measurement (which allows the acquisition of isotropic voxels)[24]. With

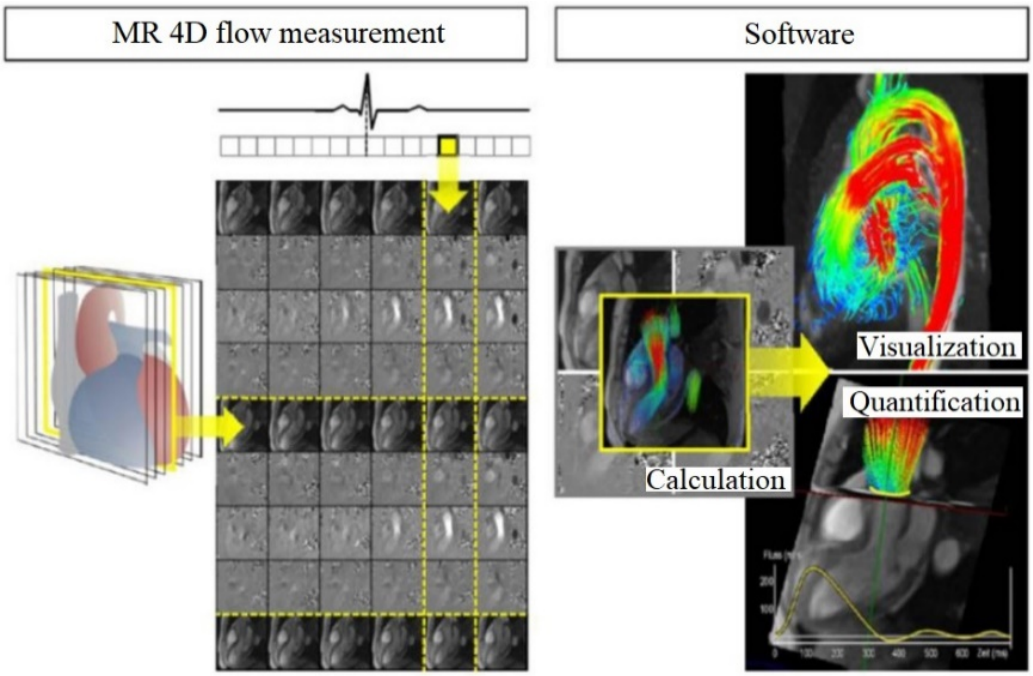

Figure 3. Workflow of a 4-D flow measurement and evaluation.
Note: A volume is covered with tridirectional (2 “in-plane” and one “through-plane” velocity) cine phase contrast measurements. Using dedicated software, the velocity field in the volume can be calculated for visualization (here in the form of color-coded streamlines) as well as for calculation of fluxes through cross-sectional areas (here, for example, through an aortic cross-section).

spatial resolution of the order of 2.5 × 2.5 × 2.5 mm^3, the coverage of the heart and temporal resolution in the range of 40–60 ms, the acquisition time using conventional parallel acquisition techniques is in the order of 10 min; however, substantial further acceleration seems possible[23]. While for a long time only prototype software was available for an adequate analysis of the dew point images of a 4-D flow measurement, different commercial solutions are now available[25]. These visualize blood flows as velocity vectors, streamlines (tangential curves to velocity vectors at a certain time) or particle paths and allow the determination of flows through arbitrary cross-sectional areas[24].

Potential applications of 4-D flow measurements are manifold. Compared to multiple 2-D flow measurements, the method is particularly attractive in the study of congenital heart disease, as measurement times are effectively shorter, shunt volumes can be quantified more accurately, and complex flow patterns can be additionally visualized[26] (**Figure 4a**). The accuracy of the determination of forward and regurgitation volumes on heart valves can also be improved compared with 2-D flow measurements, because the cross-sectional areas through which the flows are determined can be adjusted retrospectively to the valve motion[24].

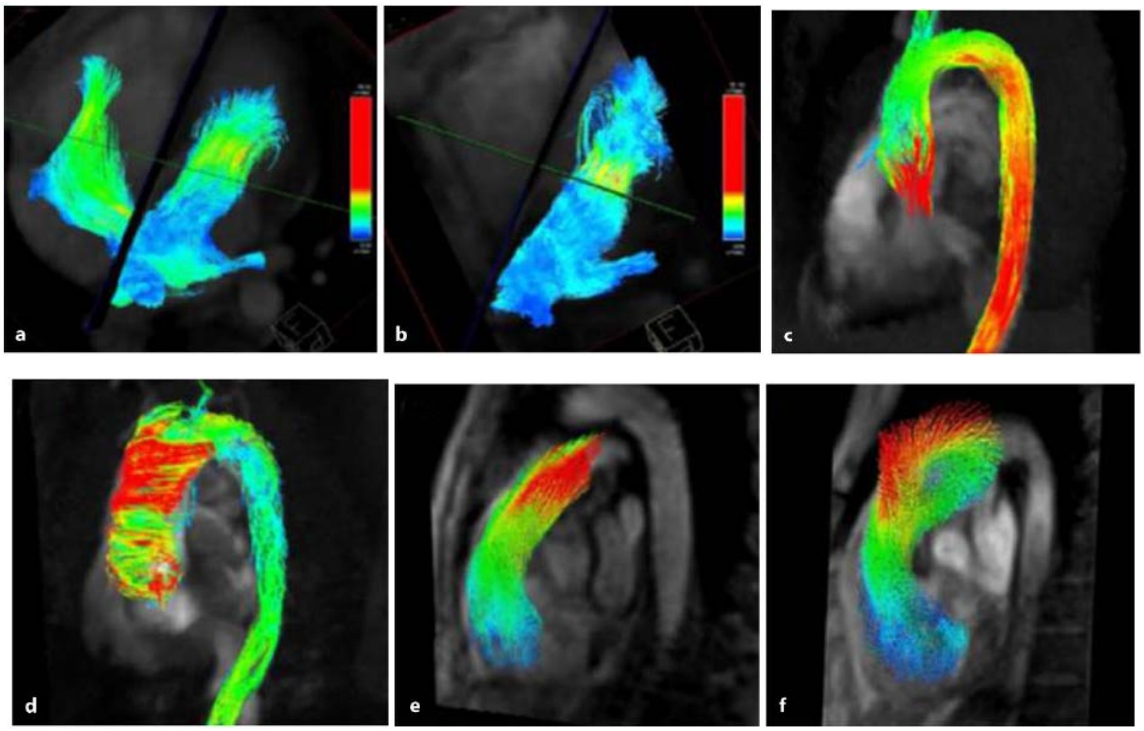

Figure 4. Flow visualizations in the case of an atrial septal defect, aortic stenosis, and pulmonary hypertension. [**a**, **b**]: particle paths running from the left to the right atrium due to an atrial septal defect (**a**), which are no longer find after closure of the atrial septal defect (**b**); [**c**, **d**]: helical systolic streamlines in a patient with aortic stenosis (**d**) compared with the more rectilinear streamlines in a healthy person (**c**); [**e**, **f**]: systolic-vortex-shaped streamlines along the main pulmonary trunk of a patient with pulmonary hypertension (**f**) compared with the rectilinear streamline in a healthy person (**e**).

In addition, hemodynamic variables derived from the velocity field could also have diagnostic and prognostic significance:

(1) Turbulent kinetic energy in the aorta can provide complementary information to echocardiography in assessing the severity of aortic valve stenosis[26]. In general, changes in the aortic valve lead to altered flow patterns (**Figure 4b**) and regional wall stresses in the aorta[26], with the latter being able to correlated with changes in the extracellular matrix of the aortic wall[27].

(2) Increased pulmonary arterial pressure leads to the occurrence of vortical flow along the main pulmonary trunk (**Figure 4c**), the duration of which can be inferred noninvasively from pulmonary arterial

pressure and the presence of pulmonary hypertonia[28].

(3) Metrics such as (turbulent) kinetic energies, hemodynamic forces, connectivity components, or even vortex formation in the cardiac chambers showed changes under systolic and diastolic dysfunction of the ventricles or in atrial ventricles[25,26]; however, their clinical relevance needs further investigation.

2.4 Functional analysis—Innovative post-processing

In the analysis of biventricular morphology and function, CMR is considered the reference standard and left ventricular ejection fraction (LVEF) is the most established marker of global myocardial function with critical implications for patient management[29]. Previous tagging-based CMR measurements were shown to be accurate in capturing regional myocardial strain, but required the acquisition of specific, additional sequences and extensive post-processing, which limit their routine use[30].

The new post-processing method of feature tracking (FT) now allows simultaneous assessment of both left ventricular ejection fraction (LVEF) and strain using standardized bSSFP cine images. After automated endo- and epicardial delineation, global longitudinal, circumferential, and radial deformation are estimated from the two- and three-dimensional displacement of small anatomical elements in all myocardial segments over the cardiac cycle[31]. Global strain values were shown to be more robust and reproducible compared to regional strain values[32]. Global-longitudinal and global-circumferential strain are considered the most consistent parameters, with global-longitudinal and circumferential strain values of –20 and –17%, respectively, generally considered pathological[31]. In patients with arrhythmogenic right ventricular dysplasia (ARVD), regional right ventricular strain values have been shown to improve the detection of substrates of ventricular tachycardia compared with the LGE technique[33]. In patients with pulmonary hypertension, right ventricular strain is a promising noninvasive alternative to assess coupling and diastolic function[34].

3. Clinical applications

3.1 Memory diseases

Cardiac MRI is playing an increasingly important role in determining the etiology of hypertrophic LV without a history of aortic valve disease or hypertension. In addition to the detection of myocardial mass, the differentiated analysis of myocardial structure has a high diagnostic and prognostic relevance. In particular, Fabry disease or cardiac involvement in the context of amyloidosis can be easily diagnosed and usually well distinguished from forms of primary hypertrophic cardiomyopathy. T1 mapping before and after contrast administration is of central importance in the diagnosis[12].

3.1.1 Fabry disease

Fabry disease is a lysosomally inherited storage disease with an α-galactosidase-A-enzyme deficiency that leads to various degrees of glycophingolipid deposition in the myocytes of the heart. LV hypertrophy (LVH) initially develops and scarring is induced via concomitant inflammatory processes. With the introduction of quantitative mapping techniques, early imaging detection of a cardiac manifestation of Fabry disease became possible, as a decrease in T1 relaxation times below 900 ms (1.5 T field strength) can be observed already in early stages of the disease. In the later course of the disease, myocardial edema becomes characteristic in conventional STIR sequences as well as on quantitative T2 maps and increasing scarring in the LGE (**Figure 2**)[35]. These processes are primarily observed preferentially in the basal lateral wall region and subsequently spread to the entire LV. In addition to the diagnosis of cardiac involvement in Fabry disease, multiparametric CMR is also suitable for monitoring the course of enzyme replacement therapy. Here, the focus is on the assessment of myocardial mass, T1 mapping for graduation of lipid deposition, and clarification of myocardial inflammation by T2 mapping[35].

3.1.2 Cardiac amyloidosis

Cardiac involvement in systemic amyloidosis

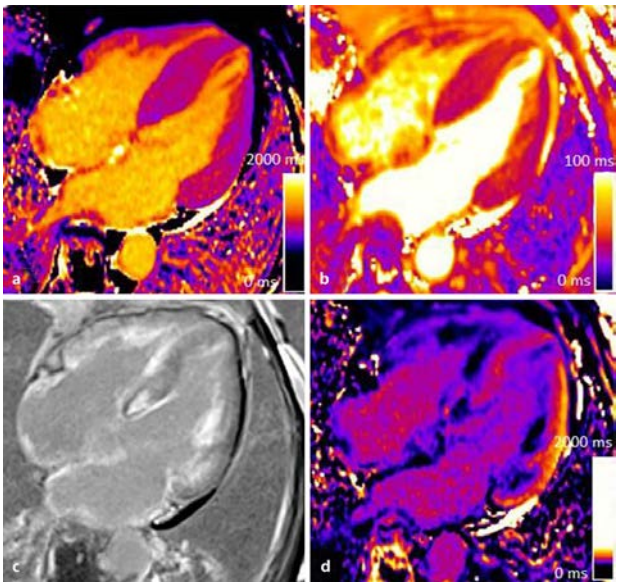

Figure 5. Cardiac ATTR amyloidosis.
Note: Cardiac MRI (magnetic resonance imaging) examination of an 80-year-old patient with condition after cardiac decompensation and intermittent atrial fibrillation; exertional dyspnea, no angina. Moderately impaired systolic pump function (left ventricular ejection fraction: 35%). N-terminal prohormone of brain natriuretic peptide (NT-proBNP) 5561 NG/L (reference range 0-486 NG/L). Endomyocardial biopsy: Congo-positive, in polarization birefringent amyloid-typical structures can be visualized. Skeletal scintigraphy with 99 mTc-3, 3-diphosphono-1, 2-propanodicarboxylic acid (Tc-99 m DPD): markedly increased global myocardial multiple enhancement. (a): 4-chamber view T1 map: globally increased T1 relaxation time 1,180 ± 38 ms. (b): 4-chamber view T2 map: globally increased T2 relaxation time 59 ± 5 ms. (c): Lower row of images on the left 4-chamber view Late gadolinium enhancement (LGE): diffuse, subendocardial focally emphasized late enhancement biventricular and biatrial. (d): 4-chamber view T1 map post-contrast: globally reduced T1 relaxation time post-contrast 312 ± 20 ms; in conjunction with the native T1 values as well as the patient's hematocrit, a formula can be used to calculate the extracellular volume (ECV), which is shown to be significantly increased in our patient at 58.4%.

is particularly common in the main forms of light chain amyloidosis (AL amyloidosis) and in the wild type (ATTR amyloidosis). In this context, the diagnosis of cardiac involvement is essential, since it is prognostic. The main goals of imaging in the work-up of a suspected cardiac amyloidosis are the subtyping of the amyloidosis and the extent of involvement. Further typing is performed by nuclear medicine using diphosphono-1,2-propanedicarboxylic acid (DPD) bone scintigraphy, which shows a sensitivity of >99% and a specificity of 86% for the detection of ATTR (wild-type) amyloidosis[36]. Patients with light chain amyloidosis typically show negative DPD bone scans as well as monoclonal gammopathy in labor tests of blood or urine[37].

Cardiac involvement in amyloidosis is due to pathological amyloid deposition in the extracellular space. In advanced stages, a restrictive phenotype with marked LVH and biatrial dilatation as well as impaired myocardial strain values is evident. The right ventricle as well as the atria may also show diffuse murine amyloid deposits. Because of these diffuse amyloid storage, myocardial nulling typically fails poorly, limiting LGE image quality, especially in late stages of disease. In the meantime, T1 mapping has become established in the field of amyloidosis assessment, both diagnostically and prognostically (**Figure 5**). T1 relaxation values are significantly elevated (>1,150 ms), especially in late disease stages; this, in combination with a restrictive CMR phenotype, effectively excludes other differential diagnoses. In addition, an increase in ECV has been established as a negative prognostic parameter with respect to survival[38]. T1 mapping and ECV as monitoring parameters in the evaluation of new therapeutic options may gain additional importance in the future.

3.2 Myocarditis/Inflammation

Acute, infectious myocarditis can be caused by a broad spectrum of pathogens, including in particular viruses (parvovirus B19, adenoviruses, cocksackie, etc.) and bacteria (e.g. Escherichia coli). Infectious myocarditis can also occur in the context of tuberculosis, autoimmune diseases or allergic events, or be caused by drugs or toxins (e.g., by immunomodulators).

CMR diagnosis of acute myocarditis has been defined by the Lake-Louise criteria since 2009, which were updated in 2018 to take the mapping technique into account[39]. In myocardial characterization by CMR, one T1- and one T2-based criteria must be met for the diagnosis of acute myocarditis (**Figure 6**). T1-based criteria derive from native T1 mapping or typical LGE as well as post-contrast T1 mapping (ECV). Characteristically, a nonischemic distribution pattern of signal changes (subendocardial recess or a noncoronary image pattern) are considered. Pathophysiologically, T1-weighted criteria represent either a hyperemia and/or a zone of

necrosis. The T2-weighted criterion as a correlate of myocardial edema and thus of acute events is derived from quantitative T2 mapping or the semi-quantitatively recorded signal intensity ratio between myocardium and skeletal muscle ≥2 in conventional T2-weighted images. The presence of pericardial effusion, pericardial thickening greater than 3 mm, or the presence of reduced ventricular function are considered supportive findings, but are not used to diagnose acute myocarditis.

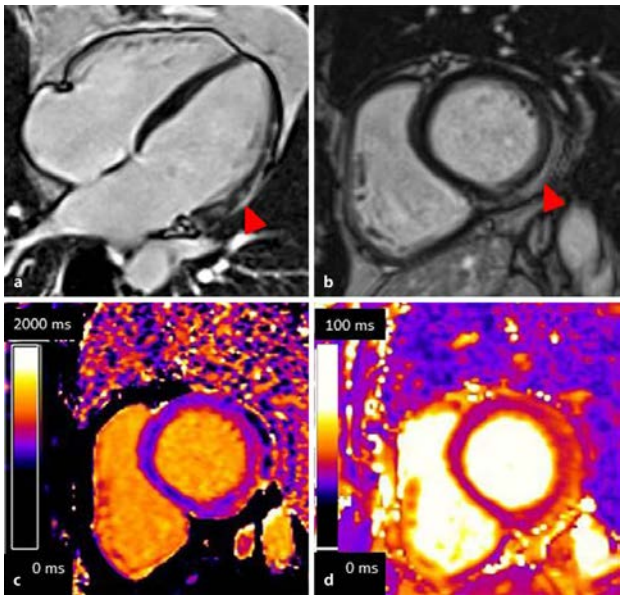

Figure 6. Myocarditis.
Note: Cardiac MRI (magnetic resonance imaging) examination of a 33-year-old patient with a new onset of impaired performance and respiratory-related chest pain after an infection of the upper respiratory tract. Highly sensitive troonin T1228NG/L (reference range: 0–14 NG/l). Endomyocardial biopsy: lymphohistiocytic myocarditis, PCR: PBV19+. (**a**, **b**): 4 Chamber view Late gadolinium enhancement (LGE) and right midventricular short axis LGE: focal patchy to streaky subepicardial late enhancement of the lateral and posterolateral walls (red arrowheads); (**c**): midventricular short axis T1 map: elevated T1 relaxation time in posterolateral region of interest (ROI) = 1,180 ms ± 38 ms, normal T1 relaxation time in septal ROI = 987 ± 35 ms; (**d**): midventricular short axis T2 map: increased T2 relaxation time in posterolateral ROI = 58 ms ± 4 ms, normal T2 relaxation time in septal ROI = 45 ± 2 ms.

The detection of acute myocarditis on cardiac MRI is not necessarily prognostic for the patient, since restitutio ad integrum may occur after the inflammation has subsided[40]. Rather, the presence of a scar in a control CMR during the interval seems to be decisive for the prognosis[41].

Subclinical forms of cardiac involvement have been demonstrated in CMR studies in numerous rheumatic systemic diseases that may be associated with generalized inflammation[42]. The criteria used for acute myocarditis cannot always be applied reliably, and the combination of clinical condition and laboratory chemistry (hs TropT, pro BNP) is seminal.

In the current COVID 19 pandemic, cardiac involvement in the context of systemic inflammation is often highly prognostic. COVID-associated myocarditis has also already been detected by CMR both in the acute stage and after passed infection[43,44]. In contrast to classical viral myocarditis, there seems to be preferential scarring in the posterior wall region after healing[43]. First studies after the disease showed that in 78% of COVID-19 patients, a myocardial involvement could be detected by CMR, which was prolonged in more than half of the cases[45].

3.3 Ischemia

In the ESC guidelines for chronic coronary artery disease (CAD) with stable angina pectoris, which were updated in 2019, a much stronger role was assigned to noninvasive imaging by computed tomography (CT), CMR, and nuclear medicine methods. Accordingly, coronary CT angiography (CTA) to exclude CAD should be performed in patients with low pretest probability. For patients with CTA or medium pretest probability, functional stress testing using CMR or equivalent nuclear medicine methods to detect relevant myocardial ischemia is suggested; evidence class IB is available in the current ESC guideline recommendations[46].

The stress CMR performed using pharmacological vasodilatation with adenosine or regadenoson or under dobutamine stress, is a long-established and standardized method for the detection of relevant myocardial ischemia. The value of stress perfusion CMR has been emphasized and expanded in recent years by several large, prospective studies. The Clinical Evaluation of Magnetic Resonance Imaging in Coronary Heart Disease (CE-MARC) study demonstrated the superiority of stress CMR compared with single-photon emission computed tomography (SPECT) in the detection of significant CHD[47].

Invasive coronary angiography was used as the gold standard, with CMR showing a higher sensitivity of 86% vs. 66.5% and also a superior negative predictive value of 90% vs. 79% compared with myocardial scintigraphy. In CE MARCII, stress CMR and scintigraphy were shown to be superior to the National Institute for Health and Care Excellence (NICE) guidelines in avoiding unnecessary invasive CHD investigations[48]. The first comparative effectiveness study MR-INFORM also showed that patient management based on noninvasive CMR stress testing was comparable to invasive intracoronary pressure measurement ("fractional flow reserve"; FFR) in patients with stable angina[49]. Stress CMR was shown to be as reliable as invasive testing in this high-risk group with an overall lower revascularization rate during the one-year observation period. In addition, the SPINS registry showed that patients with negative stress CMR and no postischemic scar had a very good 5-year prognosis with a low cardiovascular event rate of 0.6%. Patients with two pathological findings showed a risk of 3.5% per year ($p < 0.0001$)[50].

Most recently, the 2020 ESC guidelines on the management of acute coronary syndromes also assigned CMR a central role in the management of myocardial infarction in nonobstructive coronary arteries (MINOCA)[51]. CMR is recommended as a critical imaging modality in all MINOCA patients without an apparent underlying cause, with a level of evidence IB, with the aim of differentiating a nonischemic and ischemic etiology.

3.4 Valve diseases

Echocardiography is the main modality in the evaluation of valve diseases due to its wide availability, cost effectiveness, and the possibility to record blood flow and anatomy simultaneously. In the context of valve diseases, CMR is mainly used to detect and quantify regurgitation volumes. Here, the measurement is performed via phase-contrast angiography in a defined plane close to the respective valve. This method is particularly well established in the initial evaluation and monitoring of aortic and pulmonary regurgitation due to its good reproducibility. In addition, associated ventricular changes in size and structure can be accurately recorded and tracked.

Data on the prognostic value of CMR detection of regurgitation fraction are currently limited[52] and restricted to adults with congenital heart disease (EMAH) in the pulmonary valve region[53]. For EMAH, the 2020 ESC guidelines recommend CMR application broadly to detect anatomy, ventricular function, flow conditions including shunt quantification, and stress CMR for congenital pathologies of the coronary arteries to detect relevant ischemia[54].

New developments, especially 4-D flow measurement, will provide further insight into hemodynamic changes associated with valve vitiation in the future. The detection of turbulent flow (e.g., in the context of pulmonary hypertension or bicuspid valves) seems to be of particular relevance[55].

4. Conclusion for practice

The range of indications for CMR (cardiac magnetic resonance imaging) has continuously expanded in recent years.

With the introduction of quantitative mapping techniques and the results of large clinical ischemia studies, the value of CMR in diagnostics and prognostics has been significantly increased.

As a result, more and more recommendations for CMR use are being incorporated into the guidelines of the major cardiology societies.

Knowledge and implementation of these guideline recommendations are essential for cardiovascular radiology.

Future technical developments such as accelerated image acquisition and post-processing analyses based on artificial intelligence will further accelerate CMR measurement times and image analysis, thus increasing patient throughput and facilitating the application of the method outside dedicated centers.

Conflict of interest

The authors declared no conflict of interest.

References

1. Busse A, Rajagopal R, Yücel S, *et al.* Cardiac

MRI—update 2020. Der Radiologe 2020; 60(1): 33–40. doi: 10.1007/s00117-020- 00687-1.
2. von Knobelsdorff-Brenkenhoff F, Schulz-Menger J. Role of cardiovascular magnetic resonance in the guidelines of the European Society of Cardiology. Journal of Cardiovascular Magnetic Resonance 2015; 18(1): 1–18.
3. Yang ACY, Kretzler M, Sudarski S, *et al.* Sparse reconstruction techniques in MRI: Methods, applications, and challenges to clinical adoption. Investigative Radiology 2016; 51(6): 349–364.
4. Otazo R, Kim D, Axel L, *et al.* Combination of compressed sensing and parallel imaging for highly accelerated first-pass cardiac perfusion MRI. Magnetic Resonance in Medicine 2010; 64(3): 767–776.
5. Usman M, Atkinson D, Odille F, *et al.* Motion corrected compressed sensing for free-breathing dynamic cardiac MRI. Magnetic Resonance in Medicine 2013; 70(2): 504–516.
6. Kim D, Dyvorne HA, Otazo R, *et al.* Accelerated phase-contrast cine MRI using k-t SPARSE-SENSE. Magnetic Resonance in Medicine 2012; 67(4): 1054–1064.
7. Iyer SK, Tasdizen T, Burgon N, *et al.* Compressed sensing for rapid late gadolinium enhanced imaging of the left atrium: A preliminary study. Magnetic Resonance Imaging 2016; 34(7): 846–854.
8. Mehta BB, Chen X, Bilchick KC, *et al.* Accelerated and navigator-gated look-locker imaging for cardiac T1 estimation (ANGIE): Development and application to T1 mapping of the right ventricle. Magnetic Resonance in Medicine 2015; 73(1): 150–160.
9. Feng L, Axel L, Chandarana H, *et al.* XD-GRASP: Golden-angle radial MRI with reconstruction of extra motion-state dimensions using compressed sensing. Magnetic Resonance in Medicine 2016; 75(2): 775–788.
10. Kramer CM, Barkhausen J, Bucciarelli-Ducci C, *et al.* Standardized cardiovascular magnetic resonance imaging (CMR) protocols: 2020 update. Journal of Cardiovascular Magnetic Resonance 2020; 22(1): 1–18.
11. Becker MAJ, Cornel JH, Van de Ven PM, *et al.* The prognostic value of late gadolinium-enhanced cardiac magnetic resonance imaging in nonischemic dilated cardiomyopathy: A review and meta-analysis. JACC: Cardiovascular Imaging 2018; 11(9): 1274–1284.
12. Messroghli DR, Moon JC, Ferreira VM, *et al.* Clinical recommendations for cardiovascular magnetic resonance mapping of T1, T2, T2* and extracellular volume: A consensus statement by the Society for Cardiovascular Magnetic Resonance (SCMR) endorsed by the European Association for Cardiovascular Imaging (EACVI). Journal of Cardiovascular Magnetic Resonance 2017; 19(1): 1–24.
13. Messroghli DR, Radjenovic A, Kozerke S, *et al.* Modified Look-Locker inversion recovery (MOLLI) for high-resolution T1 mapping of the heart. Magnetic Resonance in Medicine 2004; 52(1): 141–146.
14. Piechnik SK, Ferreira VM, Dall'Armellina E, *et al.* Shortened Modified Look-Locker Inversion recovery (ShMOLLI) for clinical myocardial T1-mapping at 1.5 and 3 T within a 9 heartbeat breathhold. Journal of Cardiovascular Magnetic Resonance 2010; 12(1): 1–11.
15. Haaf P, Garg P, Messroghli DR, *et al.* Cardiac T1 mapping and extracellular volume (ECV) in clinical practice: A comprehensive review. Journal of Cardiovascular Magnetic Resonance 2017; 18(1): 1–12.
16. Schulz-Menger J, Bluemke DA, Bremerich J, *et al.* Standardized image interpretation and post-processing in cardiovascular magnetic resonance—2020 update. Journal of Cardiovascular Magnetic Resonance 2020; 22(1): 1–22. doi: 10.1186/s12968-020-00610-6.
17. Martinez-Naharro A, Kotecha T, Norrington K, *et al.* Native T1 and extracellular volume in transthyretin amyloidosis. JACC: Cardiovascular Imaging 2019; 12(5): 810–819.
18. Sado DM, Flett AS, Banypersad SM, *et al.* Cardiovascular magnetic resonance measurement of myocardial extracellular volume in health and disease. Heart 2012; 98(19): 1436–1441
19. McAlindon E, Pufulete M, Lawton C, *et al.* Quantification of infarct size and myocardium at risk: Evaluation of different techniques and its implications. European Heart Journal-Cardiovascular Imaging 2015; 16(7): 738–746.
20. McAlindon EJ, Pufulete M, Harris JM, *et al.* Measurement of myocardium at risk with cardiovascular MR: Comparison of techniques for edema imaging. Radiology 2015; 275(1): 61–70.
21. Giri S, Shah S, Xue H, *et al.* Myocardial T2 mapping with respiratory navigator and automatic nonrigid motion correction. Magnetic Resonance in Medicine 2012; 68(5): 1570–1578.
22. von Knobelsdorff-Brenkenhoff F, Prothmann M, Dieringer MA, *et al.* Myocardial T1 and T2 mapping at 3 T: Reference values, influencing factors and implications. Journal of Cardiovascular Magnetic Resonance 2013; 15(1): 53.
23. Nayak KS, Nielsen JF, Bernstein MA, *et al.* Cardiovascular magnetic resonance phase contrast imaging. Journal of Cardiovascular Magnetic Resonance 2015; 17(1): 1–26.
24. Dyverfeldt P, Bissell M, Barker AJ, *et al.* 4D flow cardiovascular magnetic resonance consensus statement. Journal of Cardiovascular Magnetic Resonance; 2015 17(1): 1–19.
25. Ha H, Kim GB, Kweon J, *et al.* Hemodynamic measurement using four-dimensional phase-contrast MRI: Quantification of hemodynamic parameters and clinical applications. Korean Journal of Radiology 2016; 17(4): 445–462.
26. Hope MD, Sedlic T, Dyverfeldt P. Cardiothoracic magnetic resonance flow imaging. Journal of Thoracic Imaging, 2013, 28(4): 217-230.
27. Guzzardi DG, Barker AJ, Van Ooij P, *et al.* Valve-related hemodynamics mediate human bicus-

pid aortopathy: Insights from wall shear stress mapping. Journal of the American College of Cardiology 2015; 66(8): 892–900.
28. Reiter G, Reiter U, Kovacs G, *et al.* Blood flow vortices along the main pulmonary artery measured with MR imaging for diagnosis of pulmonary hypertension. Radiology 2015; 275(1): 71–79.
29. Ibanez B, James S, Agewall S, *et al.* 2017 ESC Guidelines for the management of acute myocardial infarction in patients presenting with ST-segment elevation: The Task Force for the management of acute myocardial infarction in patients presenting with ST-segment elevation of the European Society of Cardiology (ESC). European Heart Journal 2018; 39(2): 119–177.
30. Salerno M. Feature tracking by CMR: A “double feature”? JACC: Cardiovascular Imaging 2018; 11(2 Part 1): 206–208.
31. Claus P, Omar AMS, Pedrizzetti G, *et al.* Tissue tracking technology for assessing cardiac mechanics: Principles, normal values, and clinical applications. JACC: Cardiovascular Imaging 2015; 8(12): 1444–1460.
32. Taylor RJ, Moody WE, Umar F, *et al.* Myocardial strain measurement with feature-tracking cardiovascular magnetic resonance: Normal values. European Heart Journal—Cardiovascular Imaging 2015; 16(8): 871–881.
33. Zghaib T, Ghasabeh MA, Assis FR, *et al.* Regional strain by cardiac magnetic resonance imaging improves detection of right ventricular scar compared with late gadolinium enhancement on a multimodality scar evaluation in patients with arrhythmogenic right ventricular cardiomyopathy. Circulation: Cardiovascular Imaging 2018; 11(9): e007546.
34. Tello K, Dalmer A, Vanderpool R, *et al.* Cardiac magnetic resonance imaging-based right ventricular strain analysis for assessment of coupling and diastolic function in pulmonary hypertension. JACC: Cardiovascular Imaging 2019; 12(11 Part 1): 2155–2164.
35. Augusto JB, Nordin S, Vijapurapu R, *et al.* Myocardial edema, myocyte injury, and disease severity in Fabry disease. Circulation: Cardiovascular Imaging 2020; 13(3): e010171.
36. Gillmore JD, Maurer MS, Falk RH, *et al.* Nonbiopsy diagnosis of cardiac transthyretin amyloidosis. Circulation 2016; 133(24): 2404–2412.
37. Dorbala S, Ando Y, Bokhari S, *et al.* ASNC/AHA/ASE/EANM/HFSA/ISA/SCMR/SNMMI expert consensus recommendations for multimodality imaging in cardiac amyloidosis: part 1 of 2—Evidence base and standardized methods of imaging. Journal of Nuclear Cardiology 2019; 26(6): 2065–2123.
38. Martinez-Naharro A, Treibel T A, Abdel-Gadir A, *et al.* Magnetic resonance in transthyretin cardiac amyloidosis. Journal of the American College of Cardiology 2017; 70(4): 466–477.
39. Ferreira VM, Schulz-Menger J, Holmvang G, *et al.* Cardiovascular magnetic resonance in nonischemic myocardial inflammation: Expert recommendations. Journal of the American College of Cardiology; 2018; 72(24): 3158–3176.
40. White JA, Hansen R, Abdelhaleem A, *et al.* Natural history of myocardial injury and chamber remodeling in acute myocarditis: A 12-month prospective cohort study using cardiovascular magnetic resonance imaging. Circulation: Cardiovascular Imaging 2019; 12(7): e008614. doi: 10.1161/CIRCIMAGING.118.008614.
41. Aquaro GD, Ghebru Habtemicael Y, Camastra G, *et al.* Prognostic value of repeating cardiac magnetic resonance in patients with acute myocarditis. Journal of the American College of Cardiology 2019; 74(20): 2439–2448.
42. Mayr A, Kitterer D, Latus J, *et al.* Evaluation of myocardial involvement in patients with connective tissue disorders: A multi-parametric cardiovascular magnetic resonance study. Journal of Cardiovascular Magnetic Resonance 2017; 18(1): 1–13.
43. Huang L, Zhao P, Tang D, *et al.* Cardiac involvement in patients recovered from COVID-2019 identified using magnetic resonance imaging. Cardiovascular Imaging 2020; 13(11): 2330–2339.
44. Inciardi R M, Lupi L, Zaccone G, *et al.* Cardiac involvement in a patient with coronavirus disease 2019 (COVID-19). JAMA Cardiology 2020; 5(7): 819–824.
45. Puntmann VO, Carerj ML, Wieters I, *et al.* Outcomes of cardiovascular magnetic resonance imaging in patients recently recovered from coronavirus disease 2019 (COVID-19). JAMA Cardiology 2020; 5(11): 1308. doi: 10.1001/jamacardio.2020.3557.
46. Knuuti J, Wijns W, Saraste A, *et al.* 2019 ESC guidelines for the diagnosis and management of chronic coronary syndromes: The task force for the diagnosis and management of chronic coronary syndromes of the European society of cardiology (ESC). European Heart Journal 2020; 41(3): 407–477.
47. Greenwood JP, Maredia N, Younger JF, *et al.* Cardiovascular magnetic resonance and single-photon emission computed tomography for diagnosis of coronary heart disease (CE-MARC): A prospective trial. The Lancet 2012; 379(9814): 453–460.
48. Greenwood JP, Ripley DP, Berry C, *et al.* Effect of care guided by cardiovascular magnetic resonance, myocardial perfusion scintigraphy, or NICE guidelines on subsequent unnecessary angiography rates: The CE-MARC 2 randomized clinical trial. Jama 2016; 316(10): 1051–1060.
49. Nagel E, Greenwood JP, McCann GP, *et al.* Magnetic resonance perfusion or fractional flow reserve in coronary disease. New England Journal of Medicine 2019; 380(25): 2418–2428.
50. Kwong RY, Ge Y, Steel K, *et al.* Cardiac magnetic resonance stress perfusion imaging for evaluation of patients with chest pain. Journal of the American College of Cardiology 2019; 74(14): 1741–1755.

51. Collet JP, Thiele H, Barbato E, *et al.* 2020 ESC guidelines for the management of acute coronary syndromes in patients presenting without persistent ST-segment elevation. European Heart Journal 2021; 42(14): 1289–1367. doi: 10.1093/eurheartj/ehaa575.
52. Kammerlander AA, Wiesinger M, Duca F, *et al.* Diagnostic and prognostic utility of cardiac magnetic resonance imaging in aortic regurgitation. JACC: Cardiovascular Imaging 2019; 12(8 Part 1): 1474–1483.
53. Cochran CD, Yu S, Gakenheimer-Smith L, *et al.* Identifying risk factors for massive right ventricular dilation in patients with repaired tetralogy of Fallot. The American Journal of Cardiology 2020; 125(6): 970–976.
54. Baumgartner H, De Backer J, Babu-Narayan SV, *et al.* 2020 ESC guidelines for the management of adult congenital heart disease. European Heart Journal 2021; 42(6): 563–645. doi: 10.1093/eurheartj/ehaa554.
55. Reiter U, Reiter G, Fuchsjäger M. MR phase-contrast imaging in pulmonary hypertension. The British Journal of Radiology 2016; 89(1063): 20150995.